Korea-Australia Rheology Journal
Vol. 18, No. 2, June 2006 pp. 41-49

Simulations of pendant drop formation of a viscoelastic liquid

Malcolm R. Davidson*, Dalton J.E. Harvie and Justin J. Cooper-White[1]
Department of Chemical and Biomolecular Engineering, The University of Melbourne, Victoria 3010, Australia.
[1]Department of Chemical Engineering, The University of Queensland, St. Lucia, Qld. 4067, Australia.
(Received August 1, 2005; final revision received February 22, 2006)

Abstract

A modified Volume-of-Fluid (VOF) numerical method is used to predict the dynamics of a liquid drop of a low viscosity dilute polymer solution, forming in air from a circular nozzle. Viscoelastic effects are represented using an Oldroyd-B model. Predicted drop shapes are compared with experimental observations. The main features, including the timing of the shape evolution and the "bead-on-a-string" effect, are well reproduced by the simulations. The results confirm published conclusions of the third author, that the deformation is effectively Newtonian until near the time of Newtonian pinch-off and that the elastic stress becomes large in the pinch region due to the higher extensional flow there.

Keywords : pendant drop, viscoelastic, volume of fluid method, interface

1. Introduction

Interfacial break-up phenomena (e.g. drop formation) are ubiquitous in industrial and domestic settings, as well as in nature. Drops forming at nozzles, jet break-up and the collapse of liquid bridges and other related problems are important examples of such phenomena, and consequently have attracted the attention of researchers over many years (Eggers, 1997). In particular, research on pendant drop formation from a nozzle under the influence of gravity has expanded rapidly in recent years (e.g. Wilkes *et al.*, 1999; Cooper-White *et al.*, 2002) since the initial investigation by Rayleigh (1899) more than a century ago.

Most studies of drop formation concern Newtonian liquids. However, in ink-jet printing, and biological assays for example, the drop fluid can be non-Newtonian in character. Many industrial inks present highly shear-thinning and even mild yield stress behaviour. Biological fluids often contain long chain molecules and can exhibit viscoelasticity. More generally, it is well known that small amounts of polymer dissolved in a liquid can produce pronounced viscoelastic behaviour. Experimental investigation of a pendant drop of viscoelastic fluid has been undertaken by Amarouchene *et al.* (2001), Cooper-White *et al.* (2002), Smolka and Belmonte (2003), Sostarecz and Belmonte (2004), and more recently by Tirtaatmadja *et al.* (2006). Numerical studies of non-Newtonian pendant drops are limited. Yildirim and Basaran (2001) used a finite element method to examine the closely related problem of the deformation and break-up of shear-thinning liquid bridges contained between two disks. Recently, the authors used a volume-of-fluid (VOF) numerical method to study the growth and pinch-off of a pendant drop of shear-thinning and yield stress fluids (Davidson and Cooper-White, 2006; Davidson *et al.*, 2004). The aim of this paper is to extend the VOF finite volume algorithm of Rudman (1998) to apply to pendant drops of a viscoelastic fluid.

VOF methods have an advantage in that they can handle fragmentation and coalescence without special treatment, unlike many other methods designed for flow with interfaces. To date there is no published example of a VOF method applied to viscoelastic fluids. Although the numerical calculation of viscoelastic single phase and steady free surface flow has received considerable attention (e.g. Tanner and Xue, 2002; Xue *et al.*, 2004; Tanner, 2002), numerical studies of corresponding transient free surface flow or two fluid flows have been few in number. An early example is Keunings (1986) who used a finite element method with deforming elements to calculate transient viscoelastic flow with a free surface. More recently, Ramaswamy and Leal (1999a, b) used a finite difference method with a boundary-fitted coordinate system to study steady viscoelastic flow of a drop in uniaxial extensional flow, and Pillapakkam and Singh (2001) used a level-set finite element code to study the transient viscoelastic deformation of drops in simple shear and pressure driven flows and of rising bubbles. Tomé *et al.*, (2002) developed a finite difference method for unsteady free surface flow of an Oldroyd-B fluid.

*Corresponding author: m.davison@unimelb.edu.au

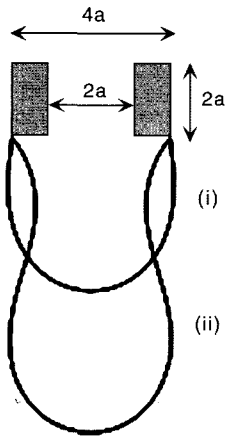

Fig. 1. Schematic showing (i) the initial drop shape and (ii) the drop shape at a later time. The shaded parts indicate the annular nozzle wall.

2. Model formulation

The growth of a pendant drop of a low viscosity dilute polymer solution forming in air from a circular nozzle (internal diameter $2a$ and external diameter $4a$) is considered. The liquid is assumed to wet the nozzle so that the liquid-air interface is attached at the outer diameter of the nozzle. The mean inflow velocity of the liquid entering the drop from the nozzle is denoted by $\bar{V}$. Axisymmetric evolution of the drop is investigated from an initial equilibrium state (Fig. 1).

In VOF methods fluid volume is advected on a fixed grid using special techniques to represent the interface within a mesh cell (Scardovelli and Zaleski, 1999). The location of the interface at any time is determined implicitly from the distribution of volume fraction. The drop and the surrounding air are considered as a single fluid with variable properties. This fluid takes the properties of the liquid within the drop and those of the air within the surroundings. The same applies when the surrounding fluid is not air, but a liquid. In that case the same polymer is assumed to be dissolved in each of the two liquids, but with different concentrations in general. Thus, if the concentration of polymer is zero then the liquid is Newtonian. Extending the assumption to cover both liquid and gas, then obviously the "polymer concentration" must be zero for a gas (e.g. air).

The Oldroyd-B viscoelastic model is chosen. This model gives constant shear viscosity and hence can be used to describe Boger fluids (typically dilute polymeric solutions). A dumbbell-based representation is used here, whereby the polymer configuration is represented by the configuration tensor $\mathbf{A} = \langle \mathbf{RR} \rangle$ where $\mathbf{R}$ is the dumbbell end-to-end vector normalised by its magnitude at equilibrum, and $\langle \mathbf{RR} \rangle$ is the ensemble average.

3. Governing equations

In terms of dimensionless velocity, length and time, scaled according to $\bar{V}$, a and $a/\bar{V}$, respectively, the equations of motion for a VOF calculation are

$$\frac{\partial \phi}{\partial t} + \nabla \cdot (\mathbf{U}\phi) = 0 \tag{1}$$

$$\frac{\partial \rho \mathbf{U}}{\partial t} + \nabla \cdot (\rho \mathbf{U}\mathbf{U}) = -\nabla P + \frac{1}{\mathrm{Fr}} \rho \hat{g} + \frac{1}{\mathrm{We}} \mathbf{F}_S + \frac{1}{\mathrm{Re}} \nabla \cdot \tau \tag{2}$$

$$\nabla \cdot \mathbf{U} = 0 \tag{3}$$

$$\frac{\partial \mathbf{A}}{\partial t} + \mathbf{U} \cdot \nabla \mathbf{A} = \mathbf{A} \cdot \nabla \mathbf{U} + (\nabla \mathbf{U})^{\mathrm{T}} \cdot \mathbf{A} - \frac{1}{\mathrm{De}} (\mathbf{A} - \mathbf{I}) \tag{4}$$

$$\tau = \mu (\nabla \mathbf{U} + (\nabla \mathbf{U})^{\mathrm{T}}) + \frac{c}{\mathrm{De}} (\mathbf{A} - \mathbf{I}) \tag{5}$$

where ϕ is a fractional volume function, P is the fluid pressure, τ is a combined viscous and elastic stress tensor, $\hat{\mathbf{g}}$ is a unit vector pointing in the direction of gravity, $\mathbf{F}_S$ is the surface force arising from interfacial effects, and c measures the concentration of dumbbells. The fractional volume function ϕ is advected with the local velocity $\mathbf{U}$. The density (ρ) and solvent shear viscosity (μ) are scaled by their values for the drop ρ_d and μ_d, respectively. The concentration of dumbbells (c) is defined as the increase in shear viscosity over that of the solvent caused by the addition of the polymer, scaled by μ_d; *i.e.* it is a dimensionless polymer contribution to the shear viscosity. The value of c within the liquid phase is denoted by c_d.

The dimensionless parameters in Equations 1-5 are the Weber, Reynolds, Froude and Deborah numbers respectively:

$$\mathrm{We} = \frac{\rho_d \bar{V}^2 a}{\sigma}, \quad \mathrm{Re} = \frac{\rho_d \bar{V} a}{\mu_d}, \quad \mathrm{Fr} = \frac{\bar{V}^2}{ga}, \quad \mathrm{De} = \frac{\bar{V} t_p}{a}. \tag{6}$$

where σ is the coefficient of interfacial tension, and t_p is the polymer relaxation time.

Realistic predictions for this problem were obtained by solving for $\mathbf{B} = c\mathbf{A}$ instead of $\mathbf{A}$. This is similar to solving directly for the elastic stress. Since the material derivative $Dc/Dt = 0$, equation 4 becomes

$$\frac{\partial \mathbf{B}}{\partial t} + \mathbf{U} \cdot \nabla \mathbf{B} = \mathbf{B} \cdot \nabla \mathbf{U} + (\nabla \mathbf{U})^{\mathrm{T}} \cdot \mathbf{B} - \frac{1}{\mathrm{De}} (\mathbf{B} - c\mathbf{I}) \tag{7}$$

and equation 5 for the stress becomes

$$\tau = \mu (\nabla \mathbf{U} + (\nabla \mathbf{U})^{\mathrm{T}}) + \frac{1}{\mathrm{De}} (\mathbf{B} - c\mathbf{I}) \tag{8}$$

The computational domain is taken to be a cylindrical region about the axis of symmetry with radius $4a$ (twice the outer radius of the nozzle) below the nozzle and radius a within the nozzle. The length of the flow domain below the nozzle is taken to be sufficient to completely contain the drop fluid for the time of the calculation ($16a$ for the

case simulated here). Predictions for Newtonian drops are insensitive to the choice of inlet velocity profile (Davidson and Cooper-White, 2006), and the same is expected here since viscoelastic effects only become important in the region of pinch-off (Cooper-White *et al.*, 2002); a parabolic velocity profile is therefore chosen at the inlet to the nozzle.

The initial conditions are chosen to be zero fluid velocity with the dumbbells having equilibrium length and orientation ($\mathbf{B} = c\mathbf{I}$). Since the equation for **B** is hyperbolic, the components must be specified at all inflow boundaries; this is achieved by solving the **B** component equations there with $\mathbf{U} \cdot \nabla \mathbf{B} = 0$, consistent with fully developed flow at the inlet. The initial equilibrium drop shape was determined in a separate flow calculation with zero inflow to the nozzle, beginning with a drop shape of known volume (a cylinder of radius $2a$ and height $2a$, capped at its base by a hemisphere of radius $2a$), as described in Davidson *et al.* (2004). Changing the initial drop shape to a hemisphere alone gave almost coincident predictions of drop shape and elastic stress once necking of the drop had begun.

4. Solution method

Axisymmetric flow calculations are performed in cylindrical polar coordinates (r, z) on a uniform staggered mesh for velocity and pressure. The fractional volume function ϕ is solved on a computational grid (termed the "fine grid") that is twice as fine as the one used for momentum and presure (termed the "standard grid"). Time integration is performed with an explicit second-order improved Euler procedure. Further details of the algorithm for solving **U**, P and ϕ are given by Rudman (1998). This section is concerned with the solution of Equation (7) for the components of the modified configuration tensor **B** which are calculated at cell centres of the standard grid.

For axisymmetric flow with zero velocity in the azimuthal direction, the components of **B** satisfy $B_{rz} = B_{zr}$, $B_{r\theta} = B_{\theta r} = B_{z\theta} = B_{\theta z} = 0$, and the equations for the non-zero components are

$$\frac{\partial B_{zz}}{\partial t} + U_r\frac{\partial B_{zz}}{\partial r} + U_z\frac{\partial B_{zz}}{\partial z} = 2B_{zz}\frac{\partial U_z}{\partial z} + 2B_{rz}\frac{\partial U_z}{\partial r} - \frac{1}{\mathrm{De}}(B_{zz} - c) \quad (9)$$

$$\frac{\partial B_{rr}}{\partial t} + U_r\frac{\partial B_{rr}}{\partial r} + U_z\frac{\partial B_{rr}}{\partial z} = 2B_{rr}\frac{\partial U_r}{\partial r} + 2B_{rz}\frac{\partial U_r}{\partial z} - \frac{1}{\mathrm{De}}(B_{rr} - c) \quad (10)$$

$$\frac{\partial B_{rz}}{\partial t} + U_r\frac{\partial B_{rz}}{\partial r} + U_z\frac{\partial B_{rz}}{\partial z} = B_{rr}\frac{\partial U_z}{\partial r} + B_{rz}\left(\frac{\partial U_r}{\partial r} + \frac{\partial U_z}{\partial z}\right) + B_{zz}\frac{\partial U_r}{\partial z} - \frac{1}{\mathrm{De}}B_{rz} \quad (11)$$

$$\frac{\partial B_{\theta\theta}}{\partial t} + U_r\frac{\partial B_{\theta\theta}}{\partial r} + U_z\frac{\partial B_{\theta\theta}}{\partial z} = 2B_{\theta\theta}\frac{U_r}{r} - \frac{1}{\mathrm{De}}(B_{\theta\theta} - c) \quad (12)$$

The advection step is performed first, using a second order upwind scheme with van Leer flux limiting (Hirsch, 2000) to limit numerical diffusion. This level of approximation is consistent with that in the momentum update.

Singh and Leal (1993) developed a numerical procedure that ensures that the diagonal components of **A** remain positive, as required for physical reasons. They found that this could be achieved numerically if one ensures that all the principal values of **A** (and hence the determinant) are positive (*i.e.* **A** must be positive definite). The same applies to **B**. In terms of **B**, the procedure involves rotating the frame of reference at each mesh point so that the local frame is oriented with the principal axes of **B**, and then splitting the update in time into implicit and explicit parts so that the updated **B** remains positive; the rotation of the frame is then reversed. Singh and Leal illustrated their procedure as a modification to the discretisation of the advection of the conformation tensor. They used a third order upwind scheme, but any suitably accurate advection scheme, such as that applied here, can be used.

In cylindrical polar coordinates, the three eigenvalues of **B** are

$$\lambda_{1,2} = \frac{1}{2}(B_{zz} + B_{rr} \pm \sqrt{(B_{zz} - B_{rr})^2 + 4B_{rz}^2}), \quad \lambda_3 = B_{\theta\theta}. \quad (13)$$

Thus it is only necessary to rotate the frame of reference locally in the (r, z) plane. The angle of rotation θ is given by

$$\sin\theta = \frac{B_{rz}}{\sqrt{(\lambda_1 - B_{rr})^2 + B_{rz}^2}} \quad (14)$$

$$\cos\theta = \frac{\lambda_1 - B_{rr}}{\sqrt{(\lambda_1 - B_{rr})^2 + B_{rz}^2}} \quad (15)$$

An iteration is performed to evaluate θ at the forward time step.

The positiveness of $B_{\theta\theta}$ after the advection update is ensured by correcting it as follows (Singh and Leal, 1993):

$$B_{\theta\theta}^{*} = \frac{B_{\theta\theta}^{n} - \min(s, 0)}{1 + \max(s, 0)/B_{\theta\theta}^{n}} \quad (16)$$

where the advection step updates $B_{\theta\theta}^{n}$ at time step n to the value $\tilde{B}_{\theta\theta}$, and $s = B_{\theta\theta}^{n} - \tilde{B}_{\theta\theta}$.

Following the advection of each component $B_{\alpha\beta}^{n}$ at time step n to an intermediate value $B_{\alpha\beta}^{*}$, the final update to time step $n+1$ from the source contribution is performed as follows:

$$B_{\alpha\beta}^{n+1} = \frac{B_{\alpha\beta}^{*} + b_{\alpha\beta}\Delta t}{1 + a_{\alpha\beta}\Delta t}, \quad \alpha, \beta = z, r \quad (17)$$

$$a_{zz} = \frac{1}{\mathrm{De}} - \min\left(2\frac{\partial U_z}{\partial z}, 0\right) - \min\left(2\frac{B_{rz}}{B_{zz}}\frac{\partial U_z}{\partial r}, 0\right) \quad (18)$$

$$b_{zz}=\frac{c}{\mathrm{De}}+\max\left(2B_{zz}\frac{\partial U_z}{\partial z},0\right)+\max\left(2B_{rz}\frac{\partial U_z}{\partial r},0\right) \quad (19)$$

$$a_{rr}=\frac{1}{\mathrm{De}}-\min\left(2\frac{\partial U_r}{\partial r},0\right)-\min\left(2\frac{B_{rz}\partial U_r}{B_{rr}\partial z},0\right) \quad (20)$$

$$b_{rr}=\frac{c}{\mathrm{De}}+\max\left(2B_{rr}\frac{\partial U_r}{\partial r},0\right)+\max\left(2B_{rz}\frac{\partial U_r}{\partial z},0\right) \quad (21)$$

$$a_{rz}=\frac{1}{\mathrm{De}}-\min\left(\frac{\partial U_r}{\partial r},0\right)-\min\left(\frac{\partial U_z}{\partial z},0\right)$$
$$-\min\left(\frac{B_{rz}\partial U_r}{B_{rr}\partial z},0\right)-\min\left(\frac{B_{rz}\partial U_z}{B_{zz}\partial r},0\right) \quad (22)$$

$$b_{rz}=B_{rz}\left(\max\left(\frac{\partial U_r}{\partial r},0\right)+\max\left(\frac{\partial U_z}{\partial z},0\right)\right)$$
$$-B_{rz}\left(\min\left(\frac{B_{rz}\partial U_r}{B_{rr}\partial z},0\right)+\min\left(\frac{B_{rz}\partial U_z}{B_{zz}\partial r},0\right)\right)+B_{rr}\frac{\partial U_z}{\partial r}+B_{zz}\frac{\partial U_r}{\partial z} \quad (23)$$

$$a_{\theta\theta}=\frac{1}{\mathrm{De}}-\min\left(\frac{2U_r}{r},0\right) \quad (24)$$

$$b_{\theta\theta}=\frac{c}{\mathrm{De}}+B_{\theta\theta}\max\left(\frac{2U_r}{r},0\right) \quad (25)$$

Partitioning the terms on the right of equations (9-12) according to equations (18-25) ensures that the determinant of **B** at timestep $n+1$ is positive to order Δt, given that it is positive at the previous step.

For numerical stability of Newtonian flows, the time step must be limited by the Courant condition, a diffusion time step, and a capillary time step (Rudman, 1998). For viscoelastic flow the time step is also limited by a Courant condition based on the speed of elastic shear and extensional waves. These can be estimated analytically by taking the time derivative of the momentum equation, substituting the equations for the relevant components of **B**, and then considering only terms having the form of a wave equation to extract the wave speed. From this, an upper estimate for the speed (w_e) of elastic waves can be determined as

$$w_e^2=\frac{2\mathrm{tr}\mathbf{B}}{\rho\mathrm{ReDe}} \quad (26)$$

The elastic time step limit is then

$$\Delta t<\min(\Delta x,\Delta y)/w_e \quad (27)$$

5. Results and discussion

Davidson *et al.* (2004) demonstrated the validity of the numerical method for predicting Newtonian pendant drop formation by comparing predicted shapes with corresponding photographic images from an experiment for which ρ_d = 1126 kg/m^3, μ_d = 0.006 Pa s, σ = 0.07 N/m. The nozzle inner radius a = 1 mm and the volumetric flow rate of liquid is 74 ml/hr, giving a mean inflow velocity $\bar{V}$ = 6.54 mm/s. The corresponding values of the dimensionless groups are Re = 1.25, We = 0.000687, Fr = 0.00437. The air/liquid ratios were taken as ρ_a/ρ_d = 0.001 and μ_a/μ_d = 0.003. The calculation was performed on a grid having 64 cells spanning the radius of the computational domain. Grid refinement tests (Davidson *et al.*, 2004) showed negligible sensitivity of predicted drop shapes to an increase in mesh density by a factor of 1.5 in each direction. The comparison between predicted and observed drop shapes is shown here in Fig. 2. The overall detail of the drop shape, including the neck and satellite drop formation, are closely reproduced.

The same nozzle geometry and flow rate has been used for experiments with low-viscosity, elastic liquids for which the drop fluid consists of a dilute solution of polyethylene oxide (PEO) in a glycerol/water mixture (Cooper-White *et al.*, 2002; Tirtaatmadja *et al.*, 2006). Here we report results of simulations, based on the Oldroyd-B rheological model and using the methods described above, of two of these experiments having qualitatively different drop behaviour. In these experiments De = 0.031 and 0.23, based on polymer relaxation times of 4.7 ms and 35 ms, respectively, as given by Tirtaatmadja *et al.* (2006).

Fig. 3 compares a simulation with the corresponding experimental results for 0.1 wt% PEO solution (molecular weight 1×10^6 g/mol) at different times (in millseconds) relative to the time (t_0) of pinch-off when PEO is absent

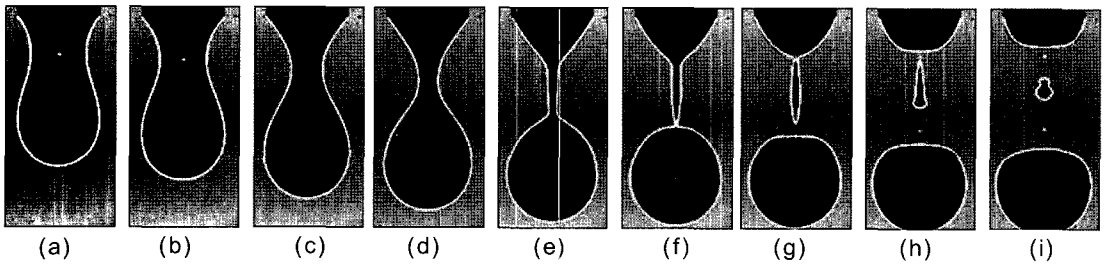

Fig. 2. Comparison between predicted drop shapes (grey outlines) and corresponding photographic images. The times in the sequence (a-i) are −30, −20, −10, −5, −1, 0, 1, 2, 3 milli-seconds, respectively, relative to the moment of pinch-off.

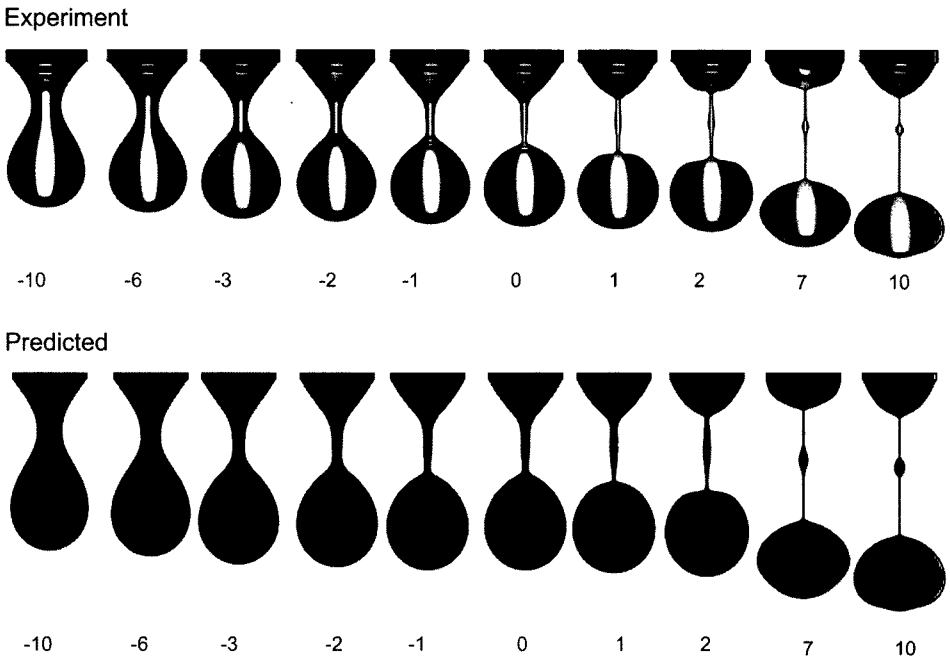

Fig. 3. Comparison between predicted drop shapes and corresponding photographic images for 0.1 wt% 10^6 g/mol PEO. The times in the sequence are in milliseconds relative to the moment of pinch-off in the case when PEO is absent and the fluid is then Newtonian.

and the fluid is then Newtonian. In this case $Re = 2.1$, $De = 0.031$ and the dumbbell concentration $c_d = 0.706$. The features of the viscoelastic deformation are well reproduced, including the timing of the evolution and the "bead-on-a-string" effect. At 7 and 10 ms the radius of the thread (defined as the radial integral of the volume function ϕ) has become smaller than the mesh spacing; consequently, quantitative predictions of thread radius at these times must be treated with caution, even though the behaviour is qualitatively correct. This limit to the resolution is manifested by the eventual numerical breaking of the thread even though a thread of an Oldroyd-B fluid should not break in finite time. This property of the Oldroyd-B model is unphysical, since the threads do break eventually in the experiments, but it only becomes important at times after the calculations are terminated.

The flow and elastic stress distributions shown in Fig. 4 illustrate the mechanism by which the elastic threads form. For $t - t_0 < 0$ (not shown in Fig. 4), the elastic stresses are sufficiently small that the flow is effectively Newtonian, as shown by Cooper-White *et al.* (2002). In this Newtonian period, the combined effects of surface tension and inertia promote necking of liquid as an approximate cylinder of small radius between the falling drop and upper liquid reservoir. At $t - t_0 \approx 0$, a pinch region forms at the lower end of this cylinder, just above the falling drop. The large surface tension forces generated by the small radius of the interface at this location increase the pressure locally within the liquid, driving fluid away from the narrowing neck. In a Newtonian fluid the thread breaks at this point as liquid is ejected both upwards and downwards away from the pinch point (see Fig. 2 at $t = t_0 = 0$ for example).

The viscoelastic and Newtonian cases differ in behaviour only once the lower pinch region has formed (compare Figs. 2 and 3). In the elastic case, the movement of fluid away from the lower pinch region at $t - t_0 \approx 0$ creates large extensional strain rates that increase the length of the polymers here. This behaviour is described by equation (4), which shows that an extensional strain rate along the centreline increases A_{zz} locally, and thus tr**A**. Indeed, Fig. 4 indicates that the magnitude of polymer extension around the lower neck region is significant, with values of tr**A** as large as 3600 being generated at the lower pinch point at $t - t_0 = 0$. This confirms the experimental conclusion of Cooper-White *et al.* (2002) that for an elastic fluid, the elastic extensional stress becomes large in the pinch region due to the higher extensional flow there.

As the polymers extend in the axial direction, so too does the elastic stress resisting the extensional strain. This is described by equations (2) and (5), which show that the elastic force increases as the gradient of tr**A** increases. The net result is that rather than the filament breaking as a Newtonian filament at the lower pinch point, the elastic stresses delay pinch-off by reducing the downwards flow out of the filament there. As the filament becomes thinner the elastic stress resists pinch-off by damping out disturbances on the surface of the thread, allowing a fine filament of droplet liquid to form whose length continues to

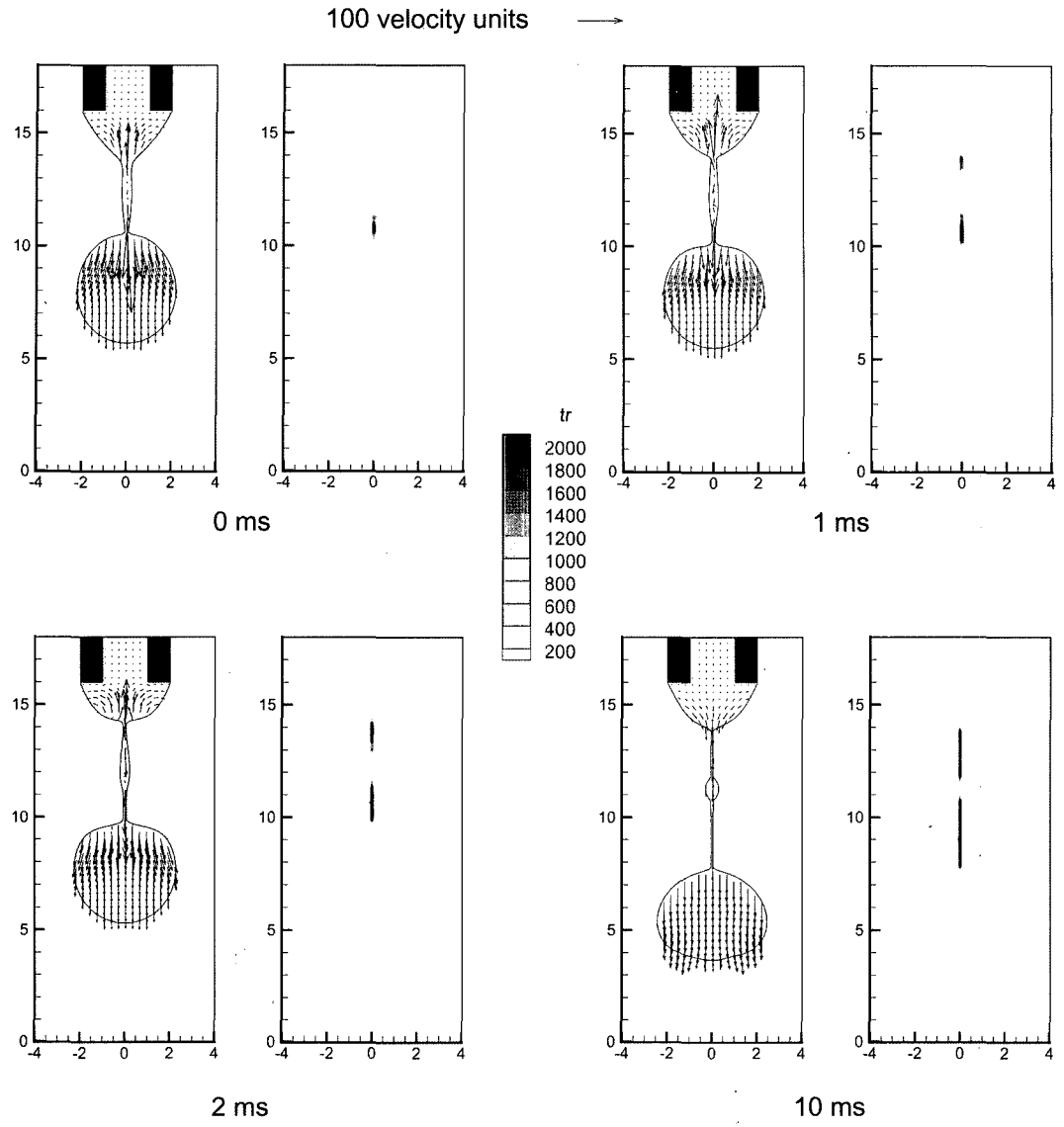

Fig. 4. Velocity field and tr**A** distribution corresponding to selected times shown in Fig. 3, relative to the time of Newtonian pinch-off.

grow as the main droplet falls. Fig. 4 shows that as the length of this filament increases, so too does the region over which tr**A** is large, in effect stabilising the filament against pinch-off. The stabilising effect of polymer has been demonstrated for the related circumstance of viscoelastic jet break-up (Christanti and Walker, 2001).

The simulation of a Newtonian drop (Fig. 2), conducted with similar nondimensional parameters to those used in the simulation of Fig. 3, shows that a separate pinch-off occurs at $t - t_0 \approx 1$ between the central fluid cylinder and upper fluid reservoir. Figs. 3 and 4 show that in the viscoelastic simulation this secondary pinch point is also initiated, but in a manner similar to that observed at the lower pinch point; *i.e.* elastic stresses resist pinch-off and allow a fine filament of fluid to form between the upper fluid reservoir and central fluid cylinder. The fluid that is now enclosed between the two pinch points at times beyond $t - t_0 = 2$ ms initially continues to drain upwards and downwards at the top and bottom pinch regions, respectively, so that the enclosed necked region contracts into a central 'bulb' and lengthening upper and lower threads. Formation of the 'bead-on-a-string' geometry, which is evident by $t - t_0 = 7$ ms, is promoted by capillary forces which act to minimise the total surface area of the liquid.

Li and Fontelos (2003) have analysed the behaviour of these 'beads-on-a-string' for Oldroyd-B fluids, and found that smaller beads slowly drain into larger beads under the action of capillary forces. Drainage occurs slowly because the elastic stresses present in the fine connecting filaments resist fluid movement. Similar behaviour is observed here. Both the experimental and simulation images of Fig. 3 show that the size of the central bead decreases slowly as

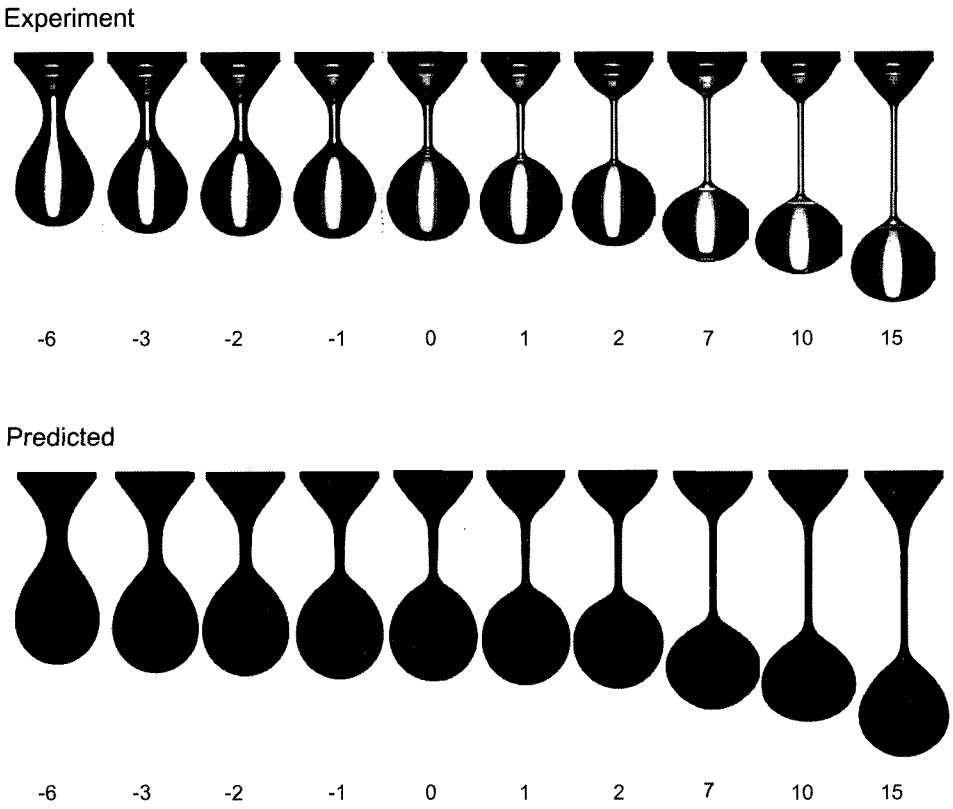

Fig. 5. Comparison between predicted drop shapes and corresponding photographic images for 0.03 wt% 5×10^6 g/mol PEO. The times in the sequence are in milliseconds relative to the moment of pinch-off in the case when PEO is absent and the fluid is then Newtonian.

time progresses. Even at $t - t_0 = 10$ ms in Fig. 4, where all velocities along the filament are directed downwards and the filament is very fine, there is a small difference in velocities between top and bottom of the central filament region that indicates that the combined volume of the bead and filament is still decreasing gradually with time.

The experiments of Cooper-White *et al.* (2002) and Tiraatmadja *et al.* (2006) show that no "bead-on-a-string" forms for large enough molecular weight of PEO solution; that is, when the solution is sufficiently elastic and the relaxation time of the polymers is large enough. Such a case is illustrated in Fig. 5 which shows measured drop shapes for 0.03 wt% 5×10^6 g/mol PEO (Tiraatmadja *et al.*, 2006) together with corresponding results of our simulation. The pattern of variation in drop shape, including the absence of bead formation, is well predicted. In this case $De = 0.23$ and the dumbbell concentration $c_d = 0.5$.

The calculated values for tr**A** for the 5×10^6 g/mol case are shown in Fig. 6. In this case tr**A** within the filament is almost an order of magnitude more than in the case of Fig. 4 as the filament between the upper liquid resevoir and lower droplet is formed. Equation (4) shows that this occurs because, for a given strain rate, the higher Deborah number means that higher A_{zz} values will be generated as the polymers relax more slowly with time. The elastic stresses inhibit the flow exiting from the filament at the top and bottom. The net result is that a thicker filament of fluid forms, with very little variation in diameter and no "bead-on-a-string". Since the filament is of almost uniform thickness, the elastic stress grows almost uniformly throughout it. In the early stages of thread formation (0 and 2 ms) fluid is ejected from the top and the bottom of the thread but at 7 and 15 ms the flow in the thread is all directed downwards. This pattern of changing velocity direction in the thread is the same for 10^6 g/mol PEO, although the transition to fully downward flow in the thread is delayed. In particular, for 10^6 g/mol, flow out of both the top and the bottom of the thread is still occurring at 7 ms, but is all directed downwards at 10 ms. The relative persistance of outflow from both ends of the thread for the 10^6 g/mol PEO occurs because the elastic stresses (which inhibit such flow) are lower than in the 5×10^6 g/mol case.

6. Conclusion

The evolution of a drop of low viscosity viscoelastic liquid forming at a circular nozzle, directed vertically downwards in air, is predicted using a Volume-of-Fluid

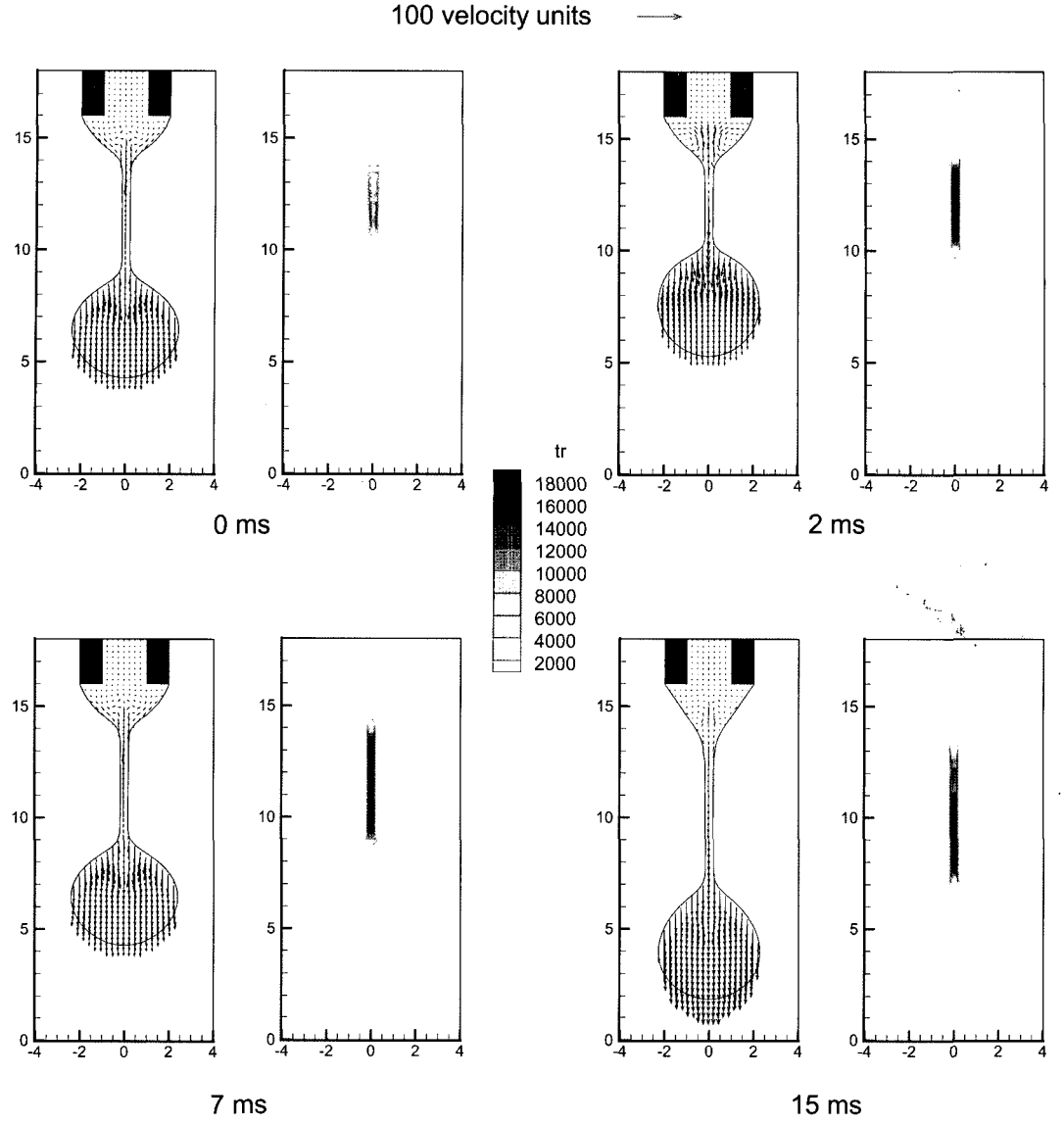

Fig. 6. Velocity field and tr**A** distribution corresponding to selected times shown in Fig. 5, relative to the time of Newtonian pinch-off.

numerical method and an Oldroyd-B model of the rheology. Results of simulations of two experiments are presented. The observed features of the viscoelastic deformation are well reproduced, including the "bead-on-a-string" effect. The predictions confirm conclusions of Cooper-White *et al.* (2002); in particular, that the deformation is effectively Newtonian until near the time of Newtonian pinch-off, and that the elastic stress does not grow by filament stretching but becomes large in the pinch region due to the higher extensional flow there.

Acknowledgement

This research was supported by an ARC Research Council grant scheme.

References

Amarouchene, Y., D. Bonn, J. Meunier and H. Kellay, 2001, Inhibition of the finite-time singularity during droplet fission of a polymeric fluid, *Phys. Rev. Lett.* **86**(16), 3558-3561.

Christanti, Y. and L. M. Walker, 2001, Surface tension driven jet break up of strain-hardening polymer solutions, *J. Non-Newtonian Fluid Mech.* **100**, 9-26.

Cooper-White, J.J., J.E. Fagan, V. Tirtaatmadja, D.R. Lester and D.V. Boger, 2002, Drop formation dynamics of constant low viscosity, elastic fluids, *J. Non-Newtonian Fluid Mech.* **106**, 29-59.

Davidson, M.R., J.J. Cooper-White and V. Tirtaatmadja, 2004, Shear-thinning drop formation, *ANZIAM J.* **45E**, part C, C405-C418.

Davidson, M.R. and J.J. Cooper-White, 2006, Pendant drop for-

mation of shear-thinning and yield stress fluids, *Appl. Math. Modelling*, in press.

Eggers, J., 1997, Nonlinear dynamics and breakup of free-surface flows, *Rev. Modern Phys.* **69**(3), 865-929.

Hirsch, C., 2000, *Numerical Computation of Internal and External Flows*, Vol. 1: Fundamentals of Numerical Discretization. Wiley.

Keunings, R., 1986, An algorithm for the simulation of transient viscoelastic flows with free surfaces, *J. Comput. Phys.* **62**, 199-220.

Li, J. and A. Fontelos, 2003, Drop dynamics on the beads-on-string structure for viscoelastic jets: A numerical study, *Phys. Fluids* **15**(4), 922-937.

Pillapakkam, S.B. and P. Singh, 2001, A level-set method for computing solutions to viscoelastic two-phase flow, *J. Comput. Phys.* **174**, 552-578.

Ramaswamy, S. and L.G. Leal, 1999a, The deformation of a viscoelastic drop subjected to steady uniaxial extensional flow of a Newtonian fluid, *J. Non-Newtonian Fluid Mech.* **85**, 127-163.

Ramaswamy, S. and L.G. Leal, 1999b, The deformation of a Newtonian drop in the uniaxial extensional flow of a viscoelastic liquid, *J. Non-Newtonian Fluid Mech.* **88**, 149-172.

Rayleigh, Lord, J.W.S., 1899, Investigations in capillarity, *Philos. Mag.* **48**, 321-337.

Rudman, M., 1998, A volume tracking method for interfacial flows with large density variations, *Int. J. Numer. Meth. Fluids* **28**, 357-378.

Scardovelli, R. and S. Zaleski, 1999, Direct numerical simulation of free-surface and interfacial flow, *Annu. Rev. Fluid Mech.* **31**, 567-603.

Singh, P. and L.G. Leal, 1993, Finite-element simulation of the start-up problem for a viscoelastic fluid in an eccentric rotating cylinder geometry using a third-order upwind scheme, *Theoret. Comput. Fluid Dynamics* **5**, 107-137.

Smolka, L.B. and A. Belmonte, 2003, Drop pinch-off and filamant dynamics of wormlike micellar fluids, *J. Non-Newtonian Fluid Mech.* **115**, 1-25.

Sostarecz, M.C. and A. Belmonte, 2004, Beads-on-string phenomena in wormlike micellar fluids, *Phys. Fluids* **16**, L67-L70.

Tanner, R.I. and S.-C. Xue, 2002, Computing transient flows with high elasticity, *Korea-Australia Rheology J.* **14**(4), 143-159.

Tanner, R.I., 2002, *Engineering Rheology*, 2nd edition, Oxford University Press.

Tirtaatmadja, V., G.H. McKinley and J.J. Cooper-White, 2006, Drop formation and breakup of low viscosity elastic fluids: Effects of molecular weight and concentration, *Phys. Fluids*, **18**, 043101.

Tomé, M.F., N. Mangiavacchi, J.A. Cuminato, A. Castelo and S. McKee, 2002, A finite difference technique for simulating unsteady viscoelastic free surface flows, *J. Non-Newtonian Fluid Mech.* **106**, 61-106.

Wilkes, E.D., S.D. Phillips and O.A. Basaran, 1999, Computational and experimental analysis of dynamics of drop formation, *Phys. Fluids* **11**(12), 3577-3598.

Xue, X.-C., R.I. Tanner and N. Phan-Thien, 2004, Numerical modelling of transient viscoelastic flows, *J. Non-Newtonian Fluid Mech.* **123**, 33-58.

Yildirim, O.E. and O.A. Basaran, 2001, Deformation and breakup of stretching bridges of Newtonian and shear-thinning liquids: Comparison of one and two-dimensional models, *Chem. Eng. Sci.* **56**, 211-233.